Development of a fiber daylighting system based on a small scale linear Fresnel reflector: Theoretical elements

A. Barbón[a], J.A. Sánchez-Rodríguez[a], L. Bayón[b,*], N. Barbón[a]

[a] *Department of Electrical Engineering, University of Oviedo, Campus of Gijón, Spain*
[b] *Department of Mathematics, University of Oviedo, Campus of Gijón, Spain*

HIGHLIGHTS

- The design of a fiber daylighting system based on a linear Fresnel reflector.
- A daylighting system like this has not been studied in the literature so far.
- This work focuses on the design of a new reflector cavity.
- The cavity used in a conventional linear Fresnel reflector is not suitable for it.
- The work presented in this paper shows the luminous energy produced per month.

ARTICLE INFO

ABSTRACT

This paper describes the details of the design of a small scale linear Fresnel reflector (*SSLFR*) applied to a daylighting system based on optical fiber bundles (*OFBs*). This study shows the influence of the *SSLFR* design parameters (mirror width, mirror length, reflector cavity height, and number of mirrors) and the parameters of the optical fiber. A new reflector cavity is designed, consisting of two right trapeziums. Each trapezium collects the incident solar irradiance of the mirrors located at each side of the central mirror. The reflector cavity has two focal points, located in the middle of the aperture of each trapezium. A MATLAB code was developed in order to obtain the optical efficiency of the new reflector cavity and numerical simulations are presented. Two *SSLFR* configurations, C_1 and C_2, are studied. C_1 is the configuration used in large-scale *LFRs* and does not consider lateral movement of the *OFBs*, as is the case in configuration C_2. Each of these configurations is analyzed considering the optimal length and longitudinal position of the *OFB*. Numerical simulations are presented for both configurations using the MATLAB environment. Power consumption based calculations are carried out using the lumen method and the potential electric energy saving is evaluated. The illumination levels obtained are then compared using the lighting design software DIAlux, a free software widely used as a planning tool by lighting designers. The results show a considerable electric energy saving with configuration C_2, although configuration C_1 also presents good energy savings.

1. Introduction

Over the last decade, global demand for artificial light has grown at an average rate of 2.4% per annum, according to the International Energy Agency (*IAE*) [1]. Annual growth was slower in *IEA* countries (1.8%) than in the rest of the world (3.6%). Globally, 133 petalumen-hours (Plmh) of electric light were consumed in 2005, an average of 20 megalumen-hours (Mlmh) of light per person, although light consumption is very unevenly distributed [1]. This growth in artificial light demand has meant that, over the last decade, global electricity consumption for lighting applications has grown at a rate of 1.5% per

annum, less than three-quarters of the light demand growth rate [1]. In view of the current socioeconomic trends and policies, global electricity consumption for lighting is projected to rise in the next 25 years to over 4250 TW h,which means an increase of 60% at an average rate of 1.9% per annum [1]. Different strategies have been proposed to reduce the energy consumption of lighting systems [2,3].

Building lighting has been the subject of special attention, as lighting represents a high percentage of the energy consumed in buildings [4,5]. It has been found that the main reason behind the increase in energy consumption is the rise in the average illuminance level. The study of the use of daylighting systems to illuminate the

Nomenclature

A_{OFB}	total *OFB* area (m²)
$A_{effecOFBi}$	effective area of the *OFB* (m²)
BPF	bundle packin fraction
B	lower side of the right trapeziums (m)
b	less side of the right trapeziums (m)
CI_m	cleanliness factor of the mirror
CI_{OFB}	cleanliness factor of the *OFB*
CR	concentration ratio
DNI	Direct Normal Irradiance (W/m²)
d	separation between two consecutive mirrors (m)
$dBloss$	attenuation (dB/km)
d_c	individual optical fiber core diameter (m)
d_{of}	individual optical fiber diameter (m)
f	distance between the OFB and the mirrors (m)
$G_{in,of}$	input irradiance solar (W/m²)
$G_{out,of}$	output irradiance solar (W/m²)
IAF	incidence angle modifier
h	depth of the air cavity (m)
K_b	luminous efficacy (Lm/W)
L	length of the individual optical fiber (km)
L_M	length of the mirrors (m)
L_{OFB}	length of the OFB (m)
L_{OFB}^l	left length of the OFB (m)
L_{OFB}^r	right length of the OFB (m)
l_{OFB}	total illuminated length of the OFB (m)
l_{OFB}^l	left illuminated length of the OFB (m)
l_{OFB}^r	right illuminated length of the OFB (m)
L_i	position of $i-th$ mirror ($0 \leq i \leq n$) (m)
N	number of individual fibers
NA	numerical aperture of the individual optical fiber
n	number of mirrors at each side of the central mirror
n_{core}	refractive index of the core
n_{clad}	refractive index of the clad
OFB	optical fiber bundle
Q_{OFB}	total power on the OFB (W)
$T(\lambda)$	transmissivity
W_M	width of the mirrors (m)
W_{ai}	width illuminated on the aperture of the reflector cavity by the i-th mirror (m)
W_{OFB}	width of the OFB (m)
α_i	angle between the vertical at the focal point and the line connecting the center point of each mirror to the focal point (°)
α_S	height angle of the Sun (°)
β_{OFB}	angle between the *OFB* and the horizontal plane (°)
β_i	tilt of $i-th$ mirror (°)
β_M	angle between the mirror axis and the horizontal plane (°)
γ	skew rays angle (°)
γ_S	azimuth of the sun (°)
η_{opt}	optical efficiency (%)
η_{SL}	solar luminaire efficiency (%)
θ_c	acceptance angle (°)
θ_{IA}	inclination angle for residential roofing (°)
θ_i	angle between the normal to the mirror and the angle of incidence of the sun (°)
θ_L	lateral incidence angle (°)
θ_l	longitudinal incidence angle (°)
θ_t	transversal incidence angle (°)
θ_z	zenith angle of the Sun (°)
λ	wavelength (nm)
μ	angle between the reflected ray and the normal to the NS axis (°)
ρ_m	reflectivity of the primary mirrors
ρ_{rc}	reflectivity of the reflector cavity
τ	transmissivity of the glass

interiors of buildings is not new [6]. Many subsequent researchers have shown that it is possible to transfer sunlight into residential buildings, in order to complement artificial lighting [7–9]. The lighting electricity savings associated with the installation of daylighting systems in buildings is estimated to be around 50–80% [10].

In addition, many authors have studied the health benefits associated with the use of daylighting [11,12], as the amount of illuminance and light quality are regarded as factors defining a healthy environment.

Daylighting systems are composed of five main elements [13]: sunlight sources, sunlight collection systems, sunlight transmission systems, lighting control systems, and solar luminaires. Sunlight collectors capture direct sunlight outside the building, sunlight distribution systems transmit sunlight to the interiors of the building, and solar luminaires distribute sunlight inside the building.

There are three main types of sunlight collectors used for daylighting: parabolic dishes, parabolic troughs, and Fresnel lenses. A parabolic dish system consists of mirrors arranged in the supporting structure to reflect and concentrate the solar radiation to the focus of the parabolic dish [14]. The parabolic dish is directed towards the sun automatically using a solar tracking mechanism, and the optical fiber is fixed permanently at the focus to collect reflected light [15,16]. In a parabolic trough system, a parabolic reflector plate is pointed at the sun with a tracking control system [17], and the optical fiber is permanently fixed at the focus of the parabolic concentrator to collect reflected light [18]. Fresnel lens refract incident sunlight to single focal pointbehind the opposite side of the lens [19], where an optical fiber or a bundle of several small fibers is mounted [20]. A comparative analysis on daylighting for parabolic dishes and Fresnel lenses has been presented by Kim et al. [21].

Light transmission systems use several devices for transmitting sunlight to the interiors of buildings: large-core optical fibers, optical fiber bundles (*OFBs*), and hollow-core reflective lightpipes. The transmission of sunlight via optical fiber is a flexible solution for daylighting systems and has a number of advantages, such as the exclusion of the ultraviolet infrared parts. An individual optical fiber is a transparent, flexible fiber with a diameter of the order of microns, consisting of a core and a clad. Core diameters range from 7 μm to 1 mm. The fiber can be made of glass or plastic. The plastic type provide more flexible solutions than the glass type, though the attenuation is greater.

The main objective of this work is to study the details of the design of a small scale linear Fresnel reflector (*SSLFR*) applied to a daylighting system based on optical fiber bundles (*OFBs*). The study makes two novel contributions.

The first being the design of a daylighting system based on *OFBs* using an *SSLFR*. To the best or our knowledge, a daylighting system with these characteristics has not yet been studied in the literature. A number of studies have been published using parabolic dishes, parabolic troughs, and Fresnel lenses refract as sunlight collectors, whereas this paper evaluates the performance of an *SSLFR* as the sunlight collector of a daylighting system. Second, the study focuses on the design of a new reflector cavity, as the cavity used in a conventional *SSLFR* is not suitable for this application. The reflector cavity proposed consists of two right trapeziums. This reflector cavity has two focal points, located in the middle of the aperture of each trapezium. The research work presented in this paper shows the luminous energy produced per month by the proposed daylighting system. In addition, an estimation of the electric energy saving and the illumination levels in a typical
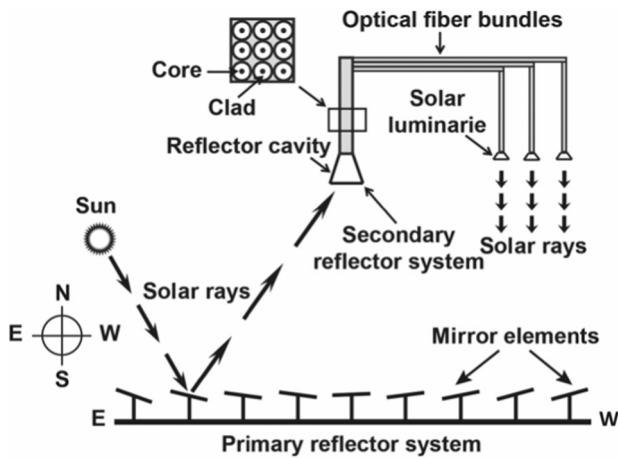
Fig. 1. Schematic of the daylighting system proposed.
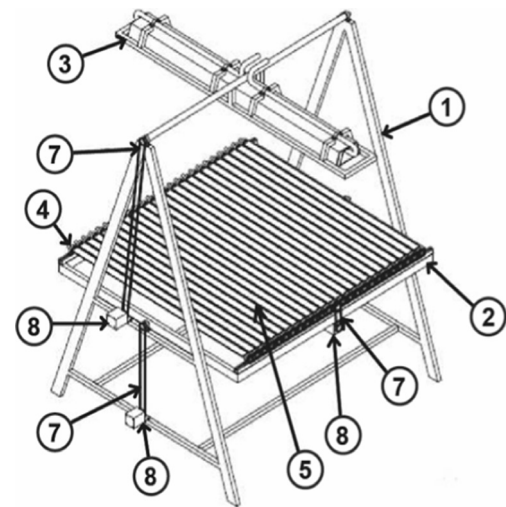
Table 1
Configurations under study.

Configuration	Mirrors		OFB	
	β_M (°)	Motion	β_{OFB} (°)	Motion
C_1	0	No	0	No
C_2	$\theta_z/2$	Yes	$\theta_z/2$	Yes

office room are presented.

The paper is organized as follows. Section 2 summarizes the main components of the daylighting system. Section 3 presents the parameters used in the transversal and longitudinal studies, the design of the reflector cavity and the calculation of the luminous flux of the daylighting system. Numerical simulations are presented in Section 4 for different configurations of the *SSLFR*. Finally, Section 5 summarizes the main contributions and conclusions of the paper.

2. Elements of the daylighting system

The main components of the proposed daylighting system are: sunlight source, *SSLFR*, *OFBs*, lighting control system, and solar luminaires. Fig.1 shows a schematic of the daylighting system proposed.

2.1. Sunlight source

Sunlight is the primary light source for daylighting systems. The Eq. (1) is used to calculate the luminous efficacy of the direct radiation (in lm/W) [22], defined as the ratio between the direct normal illuminance and the direct normal irradiance:

$$K_b = \frac{E_{bn}}{DNI} = \frac{K_m \cdot \int_{380\,nm}^{780\,nm} G_\lambda \cdot V_\lambda \cdot d\lambda}{\int G_\lambda \cdot d\lambda} \tag{1}$$

where E_{bn} is the direct normal illuminance (in lm/m² or *lx*), *DNI* is the direct normal irradiance (in W/m²), K_m is the luminous efficacy constant for photopic vision (in lm/W), G_λ is the spectral irradiance, V_λ is the spectral sensitivity of the eye, and λ is the wavelength (in nm). V_λ is defined by the numerical values given in Table 1 of [23]. For monochromatic light with a wavelength of 555 nm, K_m has a value of 683 lm/W [23].

Several luminous efficacy models based on simultaneous illuminance and irradiance measurements have been developed [24,25]. Luminous efficacy can be expressed as a function of solar altitude [26,27]. Most researchers have proposed polynomial models of different degrees for calculating K_b [28,29]. According to Darula et al. [30], each region has its own constant of luminous efficacy.

Fig. 2. Computer visualization of an SSLFR with three movements.

In this study we will use a technique which consists in the use of a single, averaged value of luminous efficacy [31]. An average value of K_b between 93 and 115 (lm/W) is suitable for beam luminous efficacy [32]. The value of 104 (lm/W), whose accuracy has been evaluated in [32], has been used by other authors [33].

2.2. SSLFR

An *SSLFR* has the configuration of a 'conventional' central *LFR*, and is composed of the following main elements: fixed structural system (1), mobile structural system (2), secondary reflector system (3), primary reflector system (4), mirror row (5), transmission means (7), and electric motors (8). The primary reflector system is composed of a row of mirrors arranged on a mobile frame. The secondary reflector system is located at a certain height from the primary reflector system and is composed of a reflector cavity in which the *OFBs* are located. This *SSLFR* has the possibility of three movements (see Fig. 2) as described in [34,35]. First, the mirrors can be rotated on the north-south axis so as to follow the sun's movement. Second, the mirror row can be rotated on the east-west axis. Finally, the receiver can also be rotated on the east-west axis. The possibility of longitudinal movement of the *SSLFR* is the main difference with respect to a large-scale *LFR*. The most important parameters of this *SSLFR* are: mirror number, mirror width, mirror length, mirror separation, and vertical distance between the mirrors and the *OFB*. These parameters are related to the rest of the elements making up the daylighting system, as will be analyzed in the following section.

2.3. Optical fiber bundles

An optical fiber bundle (*OFB*) is composed of tens to thousands of individual optical fibers, which are surrounded by epoxy glue as the filling. Therefore, there are optical losses associated with each individual optical fiber (attenuation and acceptance angle) and optical losses associated with the bundles (scattered and absorbed in the epoxy glue).

Theoretically, the attenuation of an individual optical fiber is dependent on light wavelength and fiber length. The transmissivity of an individual optical fiber is given by [36]:

$$T(\lambda) = \frac{G_{out,of}}{G_{in,of}} = 10^{\frac{-L \cdot dBloss}{10}} \tag{2}$$

where $T(\lambda)$ is the transmissivity for a specific wavelength (λ), $G_{out,of}$ is the output solar irradiance (W/m²), $G_{in,of}$ is the input solar irradiance (W/m²), L is the fiber length (km), and *dBloss* is the attenuation at each

wavelength (dB/km) or loss per kilometer. The individual optical fiber used in this study has an attenuation of 12 (dB/km) at 808 (nm) (manufacturer data).

There are also losses associated with the incidence angle of sunlight in the individual optical fiber. The total internal reflection depends on the numerical aperture, which is given by [37]:

$$NA = \sin\theta_c = (n_{core}^2 - n_{clad}^2)^{\frac{1}{2}} \tag{3}$$

where NA is the numerical aperture, θ_c is the acceptance angle, n_{core} is the refractive index of the core, and n_{clad} is the refractive index of the clad. In theory, sunlight is transmitted efficiently if the incidence angles are smaller than or equal to the acceptance angle. However, this affirmation is not completely true due to the presence of intrinsic and extrinsic attenuation losses [36]. The Eq. (3) is valid for meridional rays, which intersect the axis of the individual optical fiber after each reflexión. Besides meridional rays, there are also skew rays, which propagate by forming a spiral around the individual optical fiber. Skew rays are three-dimensional rays, whereas meridional rays propagate in a two-dimensional plane [37]. For skew rays the numerical aperture is given by [37]:

$$NA = \sin\theta_c = \frac{(n_{core}^2 - n_{clad}^2)^{\frac{1}{2}}}{\cos\gamma} \tag{4}$$

where γ is the reflection angle for skew rays within the individual optical fiber. Since $\cos\gamma$ is < 1, the acceptance angle is higher for skew rays. Therefore, the expression for NA given in Eq. (3) for meridional rays is more restrictive and, for this reason, we will consider all the sunlight as meridional rays. Moreover, the manufacturing process of an individual optical fiber should also be taken into account. This process is imperfect and hence a small fraction of sunlight is absorbed in the cladding [38].

The sunlight will only be transmitted by the core area of every individual optical fiber forming the bundle. The sunlight that foes not affect the core area will be scattered in the cladding material or absorbed in the epoxy material. The useful area of the bundle can be determined from the bundle packing fraction (BPF) [39]:

$$BPF = \frac{N \cdot \pi \cdot d_c^2}{4 \cdot A_{OFB}} \tag{5}$$

where N is the number of individual fibers, d_c is the fiber core diameter and A_{OFB} is the total bundle area.

2.4. Solar luminaries

The effective utilization of natural light inside buildings depends on the solar luminaires. A solar luminaire is an optical element designed to diffuse light with a uniform illuminance level at the working plane. A solar luminaire has to minimize transmission losses and glare, and maximize the use of available light [40]. There are two types of solar luminaires: passive and hybrid. Besides distributing direct sunlight, hybrid solar luminaires are also equipped with electric lamps. A solar luminaire is made of materials such as purified silica glass or a synthetic polymer called Poly(methyl methacrylate) or PMMA. The efficiency of a solar luminaire, η_{SL}, can be around 80% [41].

2.5. Lighting control system

Hybrid solar luminaires are equipped with dimmable electric lamps and a photocell that supplement natural light in order to compensate for these fluctuations in the intensity of collected sunlight [42]. These fluctuations are caused by changing cloud coverage or solar collector movement. A good lighting control must quickly compensate for these fluctuations, maintaining a constant level of illuminance [43]. The lighting control system will not be studied in this paper.

3. Design of the SSLFR

The calculation of the Sun's position is required in order to determine the annual output of the daylighting system. The position of the Sun can be calculated using an implementation of the Solpos algorithm [44]. This algorithm calculates, as a function of location and local time, the solar angles: height angle of the sun (α_S), zenith angle of the sun (θ_z), and azimuth of the sun (γ_S). These angles are needed to calculate the angle of incidence of solar radiation. Considering an SSLFR aligned horizontally and aligned in a North–South orientation, the angle of incidence of solar radiation will be calculated in two projection planes: the transversal incidence angle (θ_t) and the longitudinal incidence angle (θ_l) [45]. These angles are related tothe transversal and longitudinal study, respectively. The transversal incidence angle (θ_t) is defined as the angle between the vertical and the projection of the sun vector on the East-West plane (the plane orthogonal to the mirror width), and the longitudinal incidence angle (θ_l) is defined as the angle between the vertical and the projection of the sun vector on the North-South plane.

3.1. Parameters used in the transversal design

The basic parameters used in the transversal study are as follows: mirror width (W_M), vertical distance between the OFB and the mirrors (f), separation between two consecutive mirrors (d), aperture of the right trapezium (B), and number of mirrors at each side of the central mirror (n). Since there are two central mirrors, one on either side of the axis of symmetry of the SSLFR, the total number of mirrors is $2n + 2$. Using these parameters, we can determine the angle between the vertical at the focal point and the line connecting the centre point of each mirror to the focal point (α_i), as well as the width illuminated on the aperture of the reflector cavity by the i-th mirror (W_{ai}). Fig. 3 shows some ofthe parameters used in the transversal study.

The angle between the vertical at the focal point and the line connecting the centre point of each mirror to the focal point (α_i) is given by:

$$\alpha_i = \arctan\left[\frac{i \cdot (W_M + d)}{f}\right]; \quad 1 \leqslant i \leqslant n \tag{6}$$

The maximum value of this angle has to be smaller than the acceptance angle of the individual optical fiber:

$$\alpha_n \leqslant \theta_c \tag{7}$$

Therefore,

$$\arctan\left[\frac{n \cdot (W_M + d)}{f}\right] \leqslant \theta_c \tag{8}$$

The parameters that most influence the design of an SSLFR are W_M and f. The value of d is determined by [34], where the authors used a method inspired by what is known as 'Mathur's method' [46,47], which calculates the appropriate value of the shift between adjacent mirrors such that shading and blocking of reflected rays are avoided. The mirror width is hence given by:

$$W_M \leqslant \frac{f \cdot \tan\theta_c}{n} - d \tag{9}$$

Applying 'Mathur's method', the relationship between W_M and d is as follows:

$$d \geq 0.075 \cdot W_M \tag{10}$$

The typical values of the numerical aperture of an individual fiber are between 0.39 and 0.6 (see [48]). Fig. 4 shows the relationship between W_M, NA, and f, for $n = 12$. For the same value of f, if the fiber has a smaller NA, W_M must be smaller. For the same value of NA, if f is larger, W_M may be larger. However, increasing f also induces competing effects, such as focusing accuracy losses, which tend to reduce the

Fig. 3. Parameters used in transversal study.
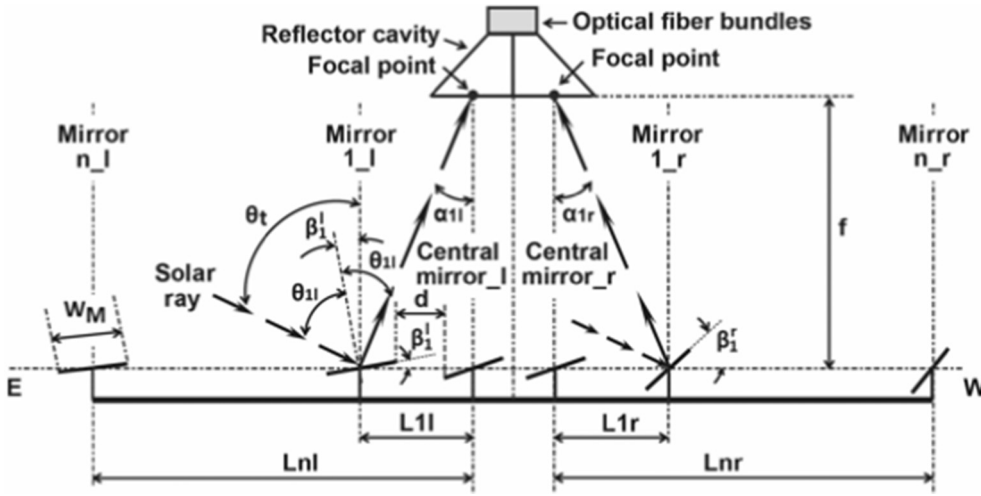
collector optical efficiency.

Fig. 5 shows the relationship between W_M, NA, and n, for $f = 1.5$ (m). For the same value of n, if the fiber has a smaller NA, W_M must be smaller. For the same value of NA, if n is smaller, W_M may be larger. Furthermore, a smaller n enables the cost of the $SSLFR$ to be decreased.

The width illuminated on the aperture of the reflector cavity by the i-th mirror (W_{ai}) can be calculated as:

$$W_{ai} = W_M \cdot [\cos\beta_i \pm \sin\beta_i \cdot \tan\alpha_i]; \quad 0 \leqslant i \leqslant n \tag{11}$$

where β_i is the tilt of the i-th mirror for $0 \leqslant i \leqslant n$. The sign $\pm$ must be adopted according to the following criteria: $-$ for the left side, and $+$ for the right side. The tilt of the central mirror (β_0) is given by:

$$\beta_0 = \frac{-\theta_t}{2} \tag{12}$$

where θ_t is the transversal incidence angle (see [45]). The tilt on the left side (β_i^l) is given by:

$$\beta_i^l = \frac{-\theta_t - \alpha_i}{2}; \quad 1 \leqslant i \leqslant n \tag{13}$$

while the tilt on the right side (β_i^r) is given by:

$$\beta_i^r = \frac{-\theta_t + \alpha_i}{2}; \quad 1 \leqslant i \leqslant n \tag{14}$$

Finally, the position of each mirror with respect to the central mirror (L_i) can be calculated as:

$$L_i = i \cdot (W_M + d); \quad 1 \leqslant i \leqslant n \tag{15}$$

3.2. Parameters used in the longitudinal design

The basic parameters used in the longitudinal study are as follows:
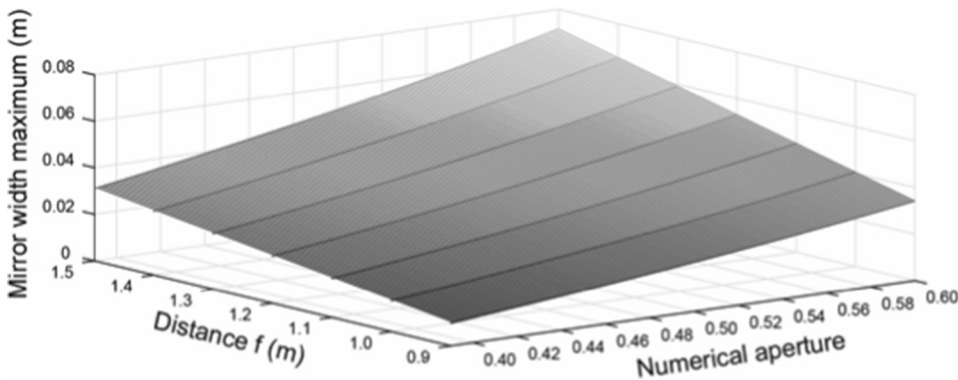
angle between the mirror axis and the horizontal plane (β_M), angle between the OFB and the horizontal plane (β_{OFB}), zenithal solar angle (θ_z), mirror length (L_M), and total length of the OFB (L_{OFB}). Fig. 6 shows the parameters used in the longitudinal study.

Due to longitudinal symmetry, we need only take into account the central mirror for the sake of this study. After some computations, we have:

$$x_0 = \frac{\left[f + \frac{L_M}{2}[\sin\beta_M - \cos\beta_M\tan\beta_{OFB}]\right]\tan\mu}{1 + \tan\beta_{OFB}\tan\mu} \tag{16}$$

and

$$x_f = \frac{\left[f + \frac{L_M}{2}[\cos\beta_M\tan\beta_{OFB} - \sin\beta_M]\right]\tan\mu}{1 + \tan\beta_{OFB}\tan\mu} \tag{17}$$

We thus define the left illuminated length of the OFB (l_{OFB}^l) as:

$$l_{OFB}^l = \frac{x_0 + \frac{L_M}{2}\cos\beta_M}{\cos\beta_{OFB}} \tag{18}$$

and the right illuminated length of the OFB (l_{OFB}^r) as:

$$l_{OFB}^r = \frac{\frac{L_M}{2}\cos\beta_M - x_f}{\cos\beta_{OFB}} \tag{19}$$

With the sign convention that we have adopted, lengths from the centre of the mirror to the left are considered positive, and those to the right, negative. The total illuminated length of the OFB (l_{OFB}) is equal to:

$$l_{OFB} = l_{OFB}^l - l_{OFB}^r \tag{20}$$

The angles β_M and β_{OFB} can take different values, while the mirrors and the OFB can have lateral movement or not. In this study, we have
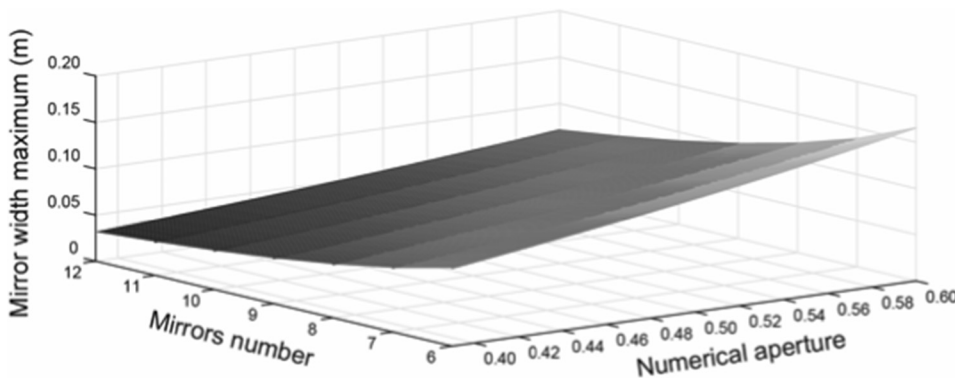
Fig. 4. Relationship between W_M, NA, and f.
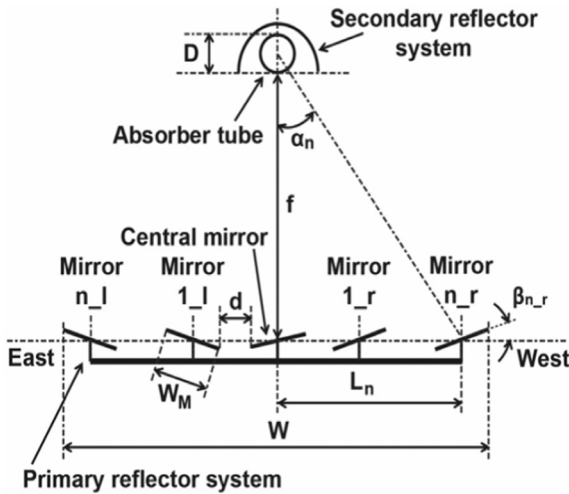
Fig. 6. Parameters used in longitudinal study.

chosen two different configurations: C_1, without longitudinal movement; and C_2, with longitudinal movement of the mirrors and the *OFB*. C_1 is the configuration used in large-scale *LFRs*, where the mirrors and the *OFB* form an angle of 0° with the horizontal plane. In configuration C_2, the rays reflected by the mirrors in the longitudinal direction are always vertical for any time of the day, varying the angle of incidence on the *OFB*. Among all the possible configurations and using the same dimensional parameters, C_2 projects the greatest amount of luminous energy on the *OFB*. Table 1 shows the main characteristics of both configurations.

The position and length of the *OFB* were calculated using the method proposed by [35], which allows obtaining the optimal values of the total length, left length, and right length of the *OFB* (L_{OFB}, L_{OFB}^l, and L_{OFB}^r respectively).

3.3. Design of the reflector cavity

There are several considerations involved in the design of the reflector cavity: optical, thermal, material and cost. The main goals of our design are: first, to maximize the optical efficiency of the reflection of the incident solar irradiance; and second, to minimize the bundle packing fraction.

The aperture of the reflector cavity must have a rectangular shape as the primary mirror field illuminates a rectangular surface on the secondary concentrator. Therefore, the proposed reflector cavity consists of two right trapeziums. Fig. 7 shows a schematic diagram of the reflector cavity, where B is the long base, b is the short base, and h is the height, i.e., the depth of the air cavity. Each trapezium collects the incident solar irradiance of the mirrors located at each side of the central mirror. The reflector cavity has two focal points, located in the

middle of the aperture of each trapezium ($B/2$). Each central mirror is focused on the focal point of each side. Thus, the main design variables are: (i) The size of the aperture of the right trapezium, B. (ii) The size of the *OFB*, b. (iii) The depth of the air cavity, h.

The design constraints are as follows: (i) B must be greater than the maximum hourly value of W_{an} (see Eq. (11)): $B > W_{an\max}$. (ii) b should be as small as possible to decrease the number of optical fibers. However, the smaller b is, the greater the possibility that the rays will bounce inside the absorber cavity and exit through the aperture. The choice of the value of b determines the value of the depth of the air cavity. (iii) h depends on the value of b. If b is smaller, h must also be smaller to ensure that all rays impinge on the *OFB*.

A MATLAB code was developed in order to trace the Sun's rays inside the reflector cavity. Ray tracing involves determining the direction of the incident rays and the point where the rays hit the cavity walls. The normal to the cavity wall at each point is also determined. The incident rays follow the law of reflection, that is, the angle of reflection equals the angle of incidence. This code calculates all the necessary optical parameters (illuminated width on the *OFB*, incidence angle on the *OFB*, and reflected rays outside of the reflector cavity), given the values of B, b and h. In Section 4, ray tracing simulations obtained with this code are presented.

The preceding study is based on the incident light rays being parallel. However, this is not the case: because of the finite angular size of the Sun's disc, the Sun's rays reaching the *OFB* are not parallel. Therefore, this consideration affects the design of the reflector cavity. In particular, it affects the calculation of the aperture of the reflector cavity. Let us consider the angular diameter of the Sun's disc, $\xi \simeq 9.3$ mrad (see Shanmugapriya et al. [49]). Fig. 8 shows that taking this parameter into consideration means that the focus width, W_{an},
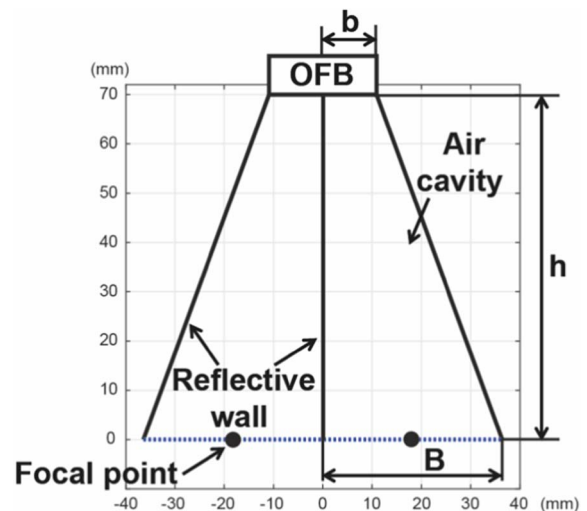
Fig. 7. Schematic diagram of the reflector cavity.
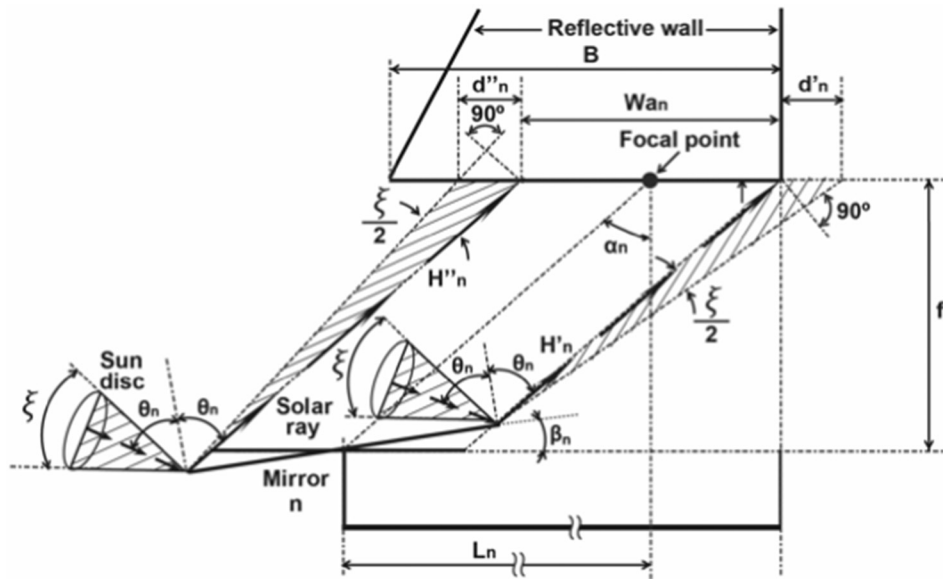
Fig. 8. Reflection of non-parallel rays.

Table 2
Values of the OFB's position and length.

Configuration	L_{OFB}^l	L_{OFB}^r	L_{OFB}
C_1	0.212	− 2.287	2.50
C_2	1.25	− 1.25	2.50

varies with respect to the value calculated in Eq. (11) with $i = n$. The illuminated area is now increased by two values that we shall call d_n' and d_n''. Their values affect the aperture of the reflector cavity.

The aim is thus to calculate the length of the lower leg of the striped, right-angled triangles in Fig. 8. To determine these distances, we straightforwardly have that:

$$H_n' = [L_n^2 + f^2]^{1/2} - \left[\left(\frac{W_M}{2} \sin(\beta_n) \right)^2 + \left(\frac{W_M}{2}\cos(\beta_n) - \frac{W_M}{2}[\cos(\beta_n) \pm \sin(\beta_n)\tan(\alpha_n)] \right)^2 \right]^{1/2}$$

(21)

$$H_n'' = [L_n^2 + f^2]^{1/2} + \left[\left(\frac{W_M}{2} \sin(\beta_n) \right)^2 + \left(\frac{W_M}{2}\cos(\beta_n) - \frac{W_M}{2}[\cos(\beta_n) \pm \sin(\beta_n)\tan(\alpha_n)] \right)^2 \right]^{1/2}$$

(22)
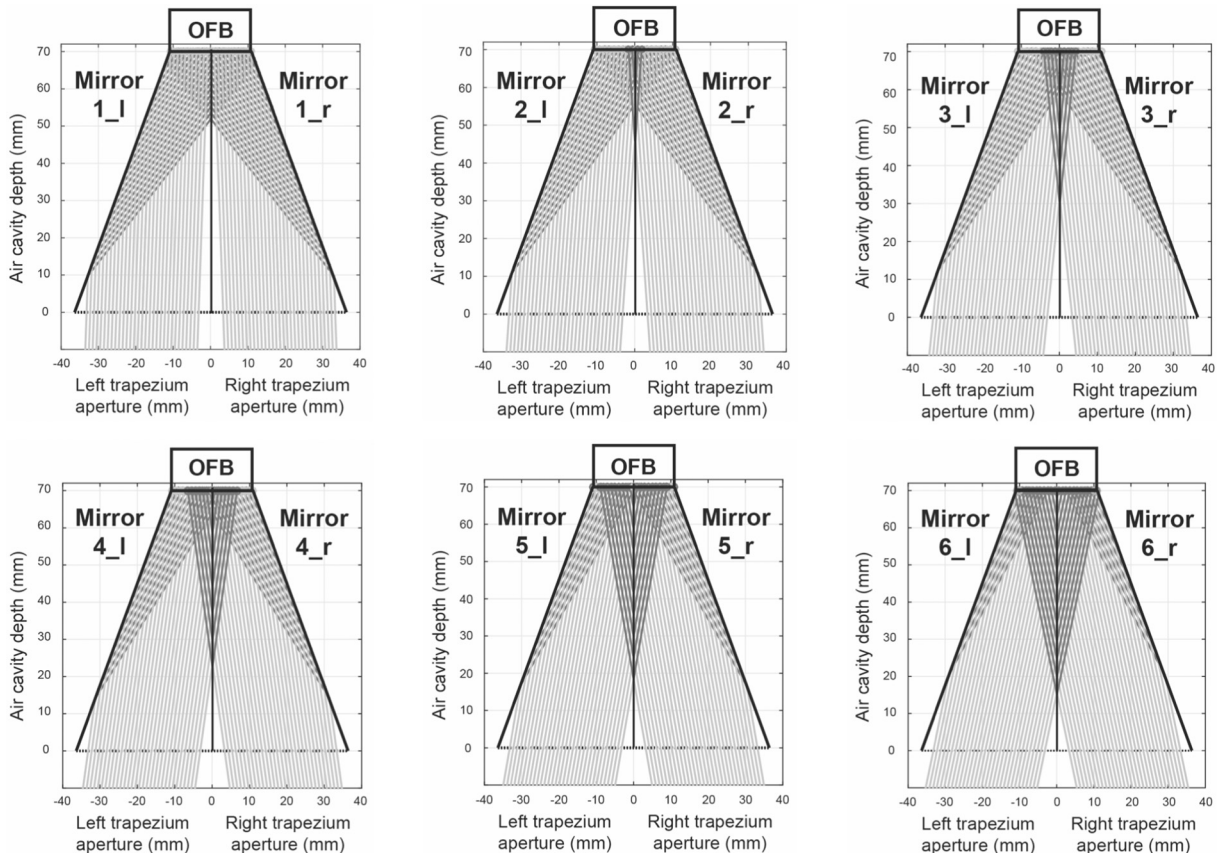
Fig. 9. Ray tracing simulations for the reflector cavity.
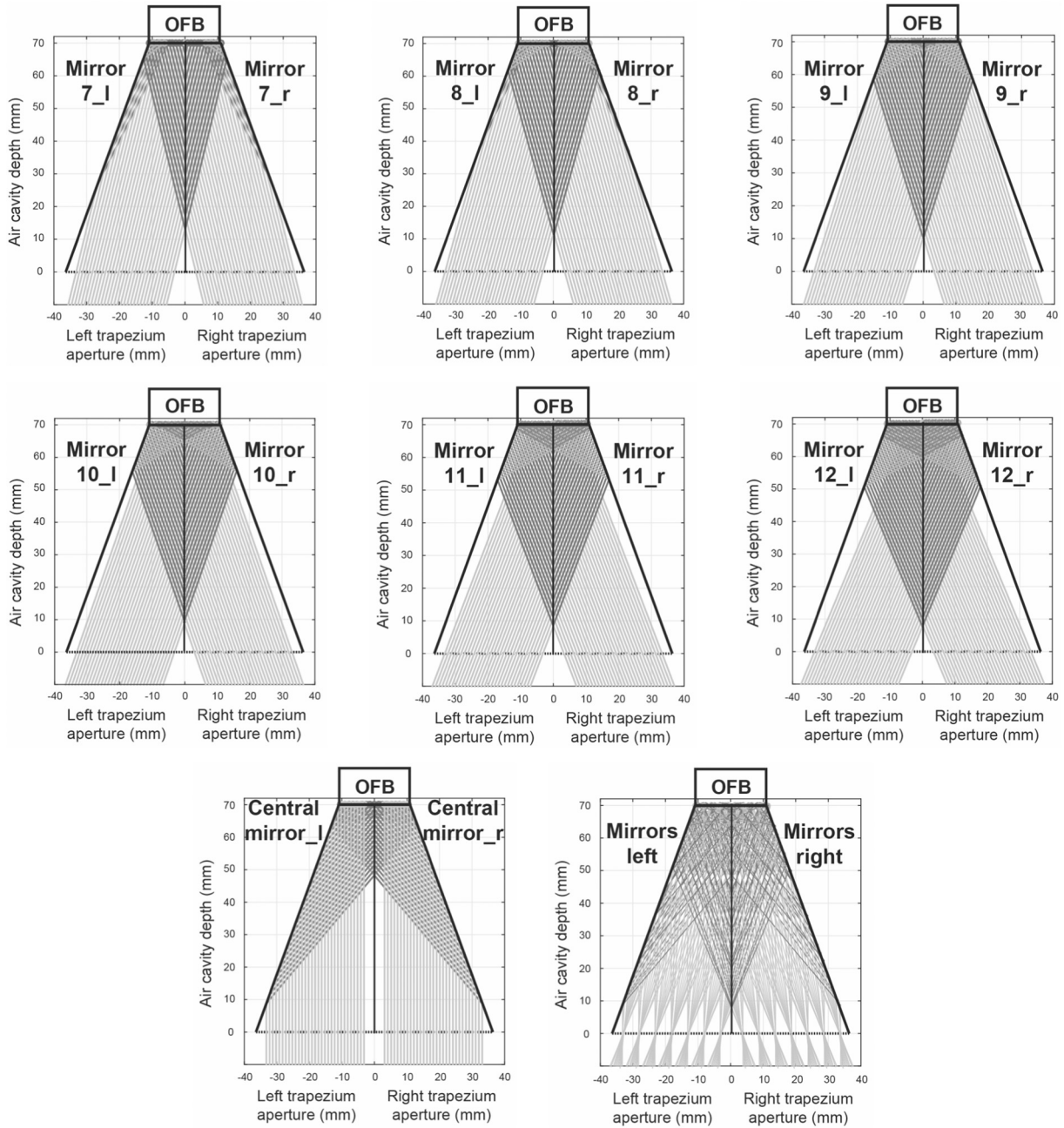
Fig. 9. (continued)

The sign $\pm$ must be adopted, once again, according to the following criteria: $^-$ for the left side, and $+$ for the right side. Hence, the distances to determine are:

$$d_n' = H_n'\tan\frac{\xi}{2}; \quad d_n'' = H_n''\tan\frac{\xi}{2} \tag{23}$$

These values of d_n' and d_n'' are then added to the previously calculated value of W_{an}.

3.4. Luminous flux of the daylighting system

The output luminous flux, Φ_{out}, can be calculated by the following expression:

$$\Phi_{out} = K_b \cdot T(\lambda) \cdot \eta_{SL} \cdot Q_{OFB} \tag{24}$$

where K_b is the luminous efficacy of the direct radiation (in lm/W), $T(\lambda)$ is the transmissivity of the individual optical fiber for a specific wavelength (λ), η_{SL} is the efficiency of the solar luminaire, and Q_{OFB} is input power on the core area of the *OFB* (in W).

The input power on the aperture of the reflector cavity will be calculated using the equation presented by [35], which is particularly suitable for the case of working with *SSLFRs*:

$$Q = 2\sum_{i=0}^{n} DNI \cdot \eta_{opt} \cdot IAF_i \cdot A_{effeci} \tag{25}$$

where:

(i) *DNI* is the direct normal irradiance.
(ii) η_{opt} is the total optical yield, which is calculated considering the reflectivity of the mirrors (ρ_m), the reflectivity of the reflector cavity(ρ_{rc}), and the cleanliness factors of the mirrors (CI_m) and the *OFB* (CI_{OFB}):

$$\eta_{opt} = \rho_m \cdot CI_m \cdot CI_{OFB} \cdot \rho_{rv} \tag{26}$$

The considered values are: $\rho_m = 0.94$, $\rho_{rv} = 0.94$ (see [50]), and $CI_m = CI_{OFB} = 0.96$ (see [51]).

(iii) IAF_i considers the variation in the optical performance of an *SSLFR* for varying ray incidence angles, which is calculated using the equation given by [34].

(iv) A_{effeci} is the effective area of the aperture of the reflector cavity that is actually illuminated by the *i*-th mirror. This area can be determined with W_{ai} and l_{OFB}:

$$A_{effeci} = W_{ai} \cdot l_{OFB}; \quad 0 \leqslant i \leqslant n \tag{27}$$

The effective area of the *OFB* that is actually illuminated by the *i*-th mirror ($A_{effecOFBi}$) can be determined as:

$$A_{effecOFBi} = CR_i \cdot A_{OFB}; \quad 0 \leqslant i \leqslant n \tag{28}$$

where A_{OFB} is the total *OFB* area, and CR_i is the concentration ratio of the *i*-th mirror, which is given by:

$$CR_i = \frac{A_{effeci}}{A_{OFB}}; \quad 0 \leqslant i \leqslant n \tag{29}$$

Therefore, the input power on the core area of the *OFB*, is given by:

$$Q_{OFB} = 2 \sum_{i=0}^{n} DNI \cdot \eta_{opt} \cdot IAF_i \cdot BPF \cdot CR_i \cdot A_{OFB} \tag{30}$$

From these equations, the output luminous flux (24) is given by:

$$\Phi_{out} = K_b \cdot T(\lambda) \cdot \eta_{SL} \cdot 2 \sum_{i=0}^{n} DNI \cdot \eta_{opt} \cdot IAF_i \cdot BPF \cdot CR_i \cdot A_{OFB} \tag{31}$$

4. Results and discussion

The assumptions made in this study are as follows:

(i) The mirrors are flat and specularly reflecting.
(ii) The rows of mirrors are perfectly tracked so as to follow the apparent movement of the Sun.
(iii) The pivoting point of each mirror coincides with its central point; hence, it is always focused on the focal point of one trapezium of the reflector cavity.

The following parameters remain constant in all the configurations:

(i) $n = 12$, considered optimal for the design of an *SSLFR* [34].
(ii) $W_M = 0.030$ (m), considered optimal for the design of an *SSLFR*, according to the method proposed by [34].
(iii) $d = 0.022$ (m). This value was obtained using a method inspired by what is known as 'Mathur's method', which calculates the appropriate value of the shift between adjacent mirrors so that shading and blocking of reflected rays are avoided, for a transversal incidence angle between −22.5° and 22.5°. In any case, the numerical simulations, performed using MATLAB, also take into account the effects of shading and blocking in those hours in which they exist.
(iv) $f = 1.5$ (m), considered optimal for the design of an *SSLFR* [34] and obtained by applying Mathur's method.
(v) $L_M = 2.5$ (m), considered optimal for the design of an *SSLFR* [34] and obtained by applying Mathur's method.
(vi) Reflector cavity parameters: $B = 0.0364$ (m), $b = 0.01092$ (m), and $h = 0.070$ (m).
(vii) L_{OFB}, L_{OFB}^l, and L_{OFB}^r, calculated according to Barbon's method [35]. These values are given in Table 2. With the sign convention that we have adopted, lengths from the centre of the mirror to the left are considered positive, and those to the right, negative. These results were obtained by setting $f = 1.5$ (m) and $L_M = 2.5$ (m).
(viii) $K_b = 104$ (lm/W) [32,33].

(ix) $d_{of} = 0.0014$ (m), taken from manufacturer data [48].
(x) $d_c = 0.001$ (m), taken from manufacturer data [48].
(xi) $dBloss = 12$ (dB/km), taken from manufacturer data [48].
(xii) $BPF = 40\%$.
(xiii) $\eta_{SL} = 80\%$ [41].
(xiv) $L = 0.010$ (km).

Using these values, α_i is less than the acceptance angle of the individual optical fiber. The study was conducted in Almeria (Spain), with latitude 36°50′07″N, longitude 02°24′08″W and altitude 22 (m). These calculations were developed by using ground-based irradiance measurement data collected at the Andalusian Energy Agency (*AAE*) [52]. The mathematical equations were implemented in a MATLAB code [53] which includes subroutines, discretized every 10 min, to calculate: *DNI*, mirror position, *IAF*, W_{ai}, and l_{OFB}. The program takes into account the effects of shading, blocking and end loss.

4.1. Ray tracing simulations

Fig. 9(a) and (b) presents ray tracing simulations for the reflector cavity. For the sake of clarity, this visualization shows a reduced number of rays. This simulation was carried out on June 21st and solar time 12:00.

4.2. Output luminous flux

Fig. 10 shows the calculation of the output luminous energy per month, for both configurations C_1 and C_2. As can be seen in this figure, configuration C_2 gives better results than configuration C_1.

4.3. Electric energy saving: a case study

A typical office room was considered in order to evaluate the electric energy saving of the daylighting system. Electric lighting is a major energy consumer in offices. The interior of an office room is organized around the needs of individual workstations which are typically 3 (m) × 3 (m) [54]. In this study, an office for 8 individual workstations is considered. The office characteristics are summarized in Table 3. The lighting system consists of a combination of daylight and electric light. Supplementary electric lighting is not used if the daylight system provides more than 500 (lx) of average illumination level. The electric
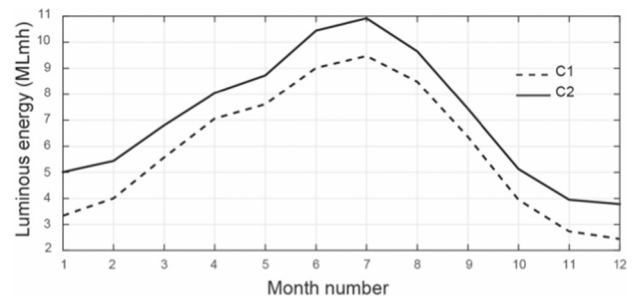
Fig. 10. The luminous energy computed for month.

Table 3
Data from the office object of study.

Data	Value
Office dimension (L × W × H)	12 (m) × 6 (m) × 3 (m)
Office reflectance ($\rho_{ceiling} \times \rho_{wall} \times \rho_{floor}$)	0.5 × 0.5 × 0.2
Other object reflectance	1.0
Height of working plane from floor	0.85 (m)
Maintenance factor	0.8
Average illumination level [55]	250–500 (lx)
Office working hours	09: 00–16: 30

Table 4
Rated values of commercial lamps [56].

Lamp type	Wattage (W)	Lumens	Rated life (h)
Fluorescent lamp (FL)	18	1350	20,000

Fig. 11. Electric saving in C_1.

Fig. 12. Electric saving in C_2.

lighting system is controlled by light sensors. The rated values of the lamps, taken from the manufacturer's catalog, are summarized in Table 4. The utilization factor of the luminaires is assumed to be 0.44, and the luminous flux delivered was calculated using the lumen method. The number of lamps is 32 and the total electric consumption is 576 (W).

The electric saving is estimated calculating the electric consumption of the combined system every 10 min, and comparing this value with the electric consumption without the daylighting system. The electric consumption of the *SSLFR* was ignored in this study, since it is very small compared to the total electric consumption.

Figs. 11 and 12 show, in percentage terms, the electric saving for both configurations C_1 and C_2, computed on June 21st (Summer solstice) and December 21st (Winter solstice). For the worst day of the year, using configuration C_1, the energy saving is higher than 20% for 5 h. On June 21st, the energy saving using configuration C_1 is higher than 50% during office working hours. For the worst day of the year, the energy saving using configuration C_2, is higher than 30% for 5 h. On June 21st, the energy saving using configuration C_2 is higher than 70% for 5 h. It is clear that configuration C_2 gives higher electric savings but at an increased capital cost for the additional motion.

Fig. 13 shows, in percentage terms, the monthly electric saving for both configurations C_1 and C_2. Obviously, the best results are obtained in the summer months. As an example, the average energy saving in July is 74.8% in configuration C_2, and 65.4% in configuration C_1. On the contrary, the average energy saving in January is 43.4% in configuration C_2, and 28.4% in configuration C_1.

This monthly analysis shows that configuration C_2 always gives higher energy savings than configuration C_1. The difference between both configurations is maximum in the central hours of the day (around 18% on average), since configuration C_2 takes better advantage of the incident radiation at daylight hours with higher solar radiation. This effect is due to the fact that, while configuration C_1 only has the transversal movement of the primary reflector system, configuration C_2 has also the possibility of longitudinal movement of the mobile structural system and the secondary reflector system. In contrast, at the first and last working hours this difference is much smaller (around 6% and 3% respectively).
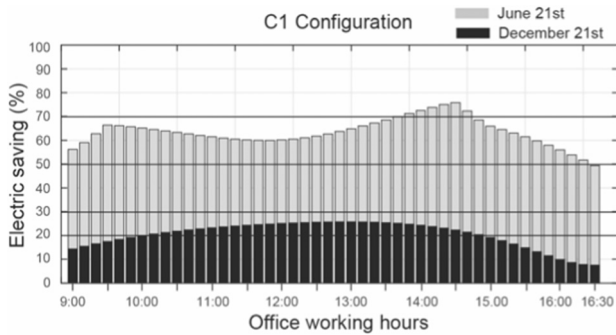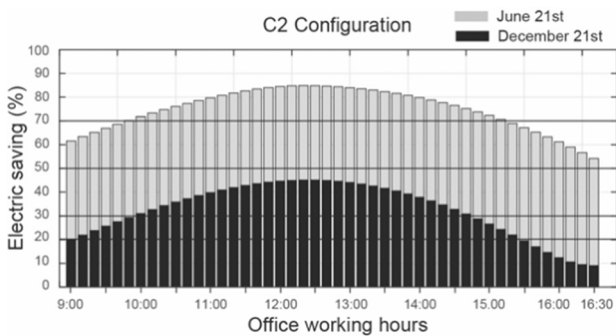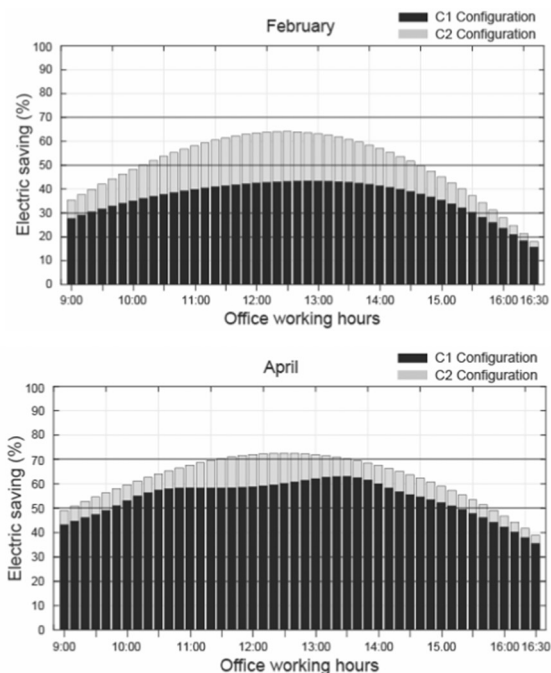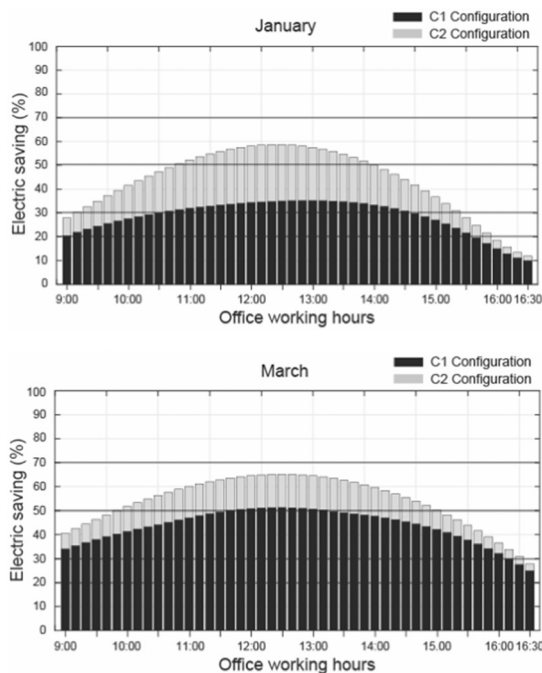
Fig. 13. (a) Percentage electric saving per month, (b) percentage electric saving per month and annual.
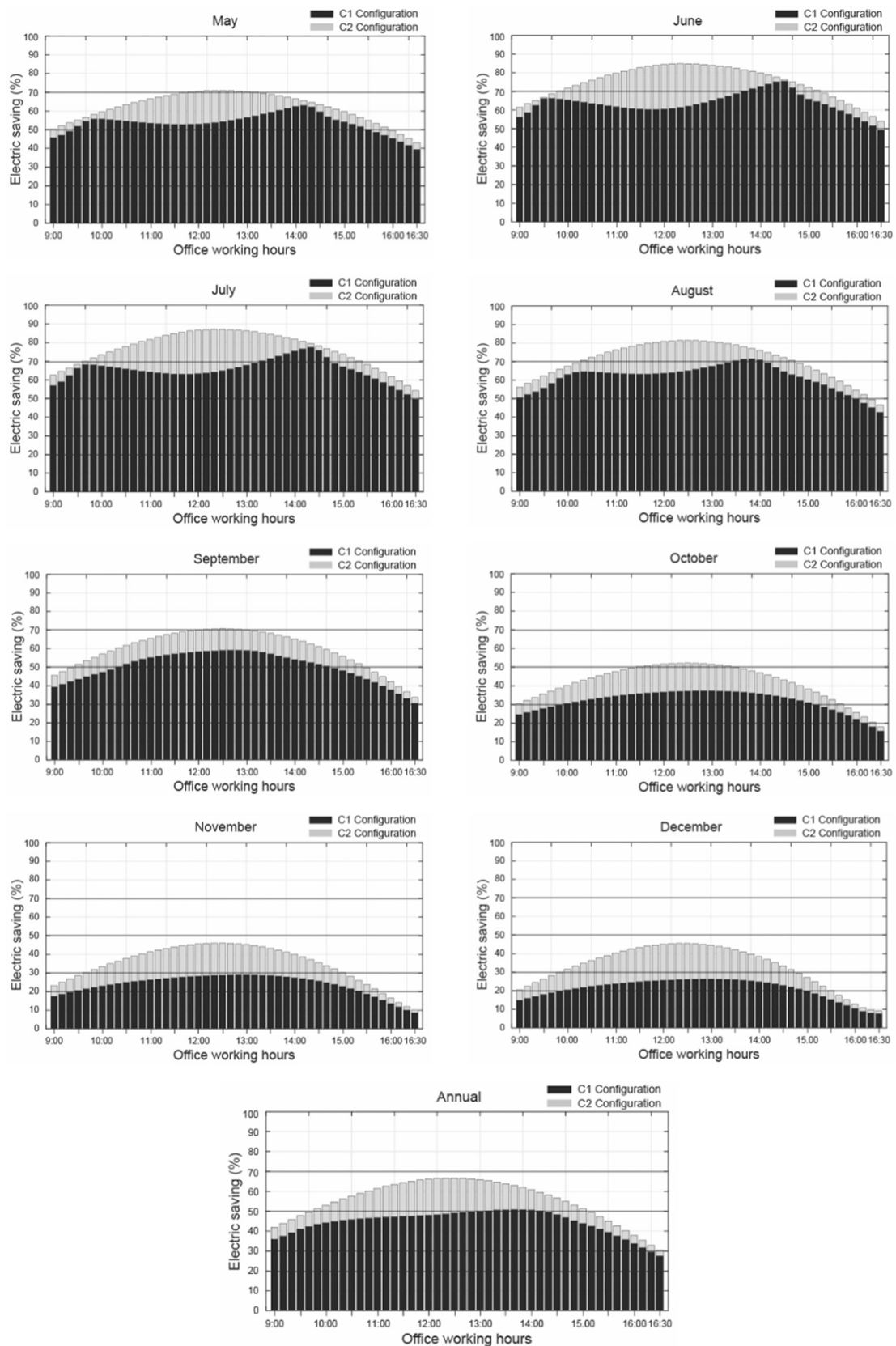
Fig. 13. (continued)

Comparing the months of the year with each other, the difference in energy savings is maximum for December-January and June-July, and minimum for March-April and September-October, since at the March and September equinoxes the Sun's declination is zero. With a declination close to zero, both configurations have similar efficiency.

The light distribution in the office room considered has been calculated using the lighting design software DIAlux [57], which is a free software widely used as a planning tool by lighting designers [58].
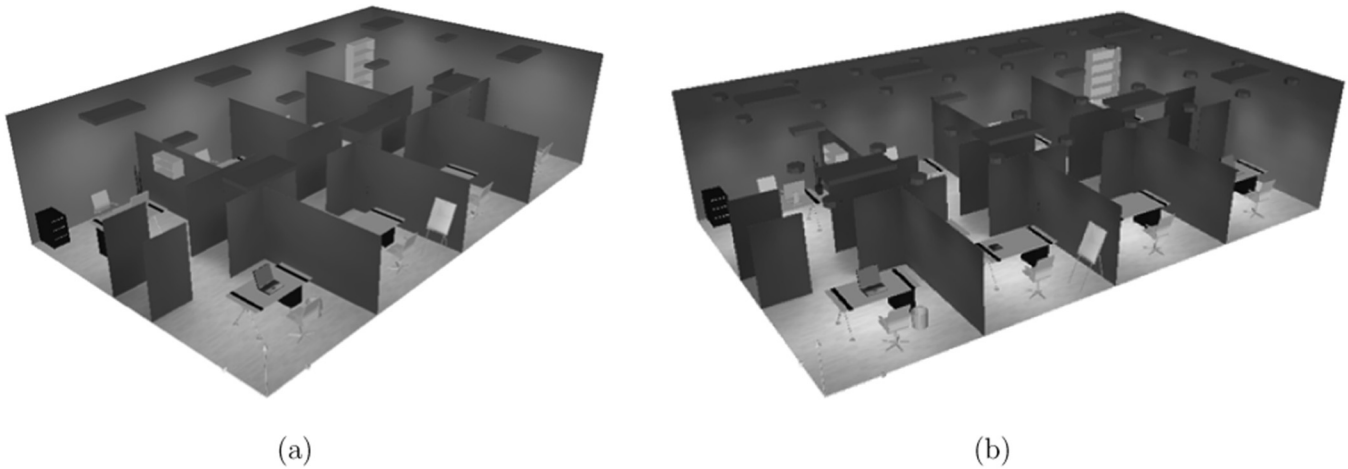
Fig. 14. Interior view of the office room: (a) artificial lighting and (b) daylighting system.
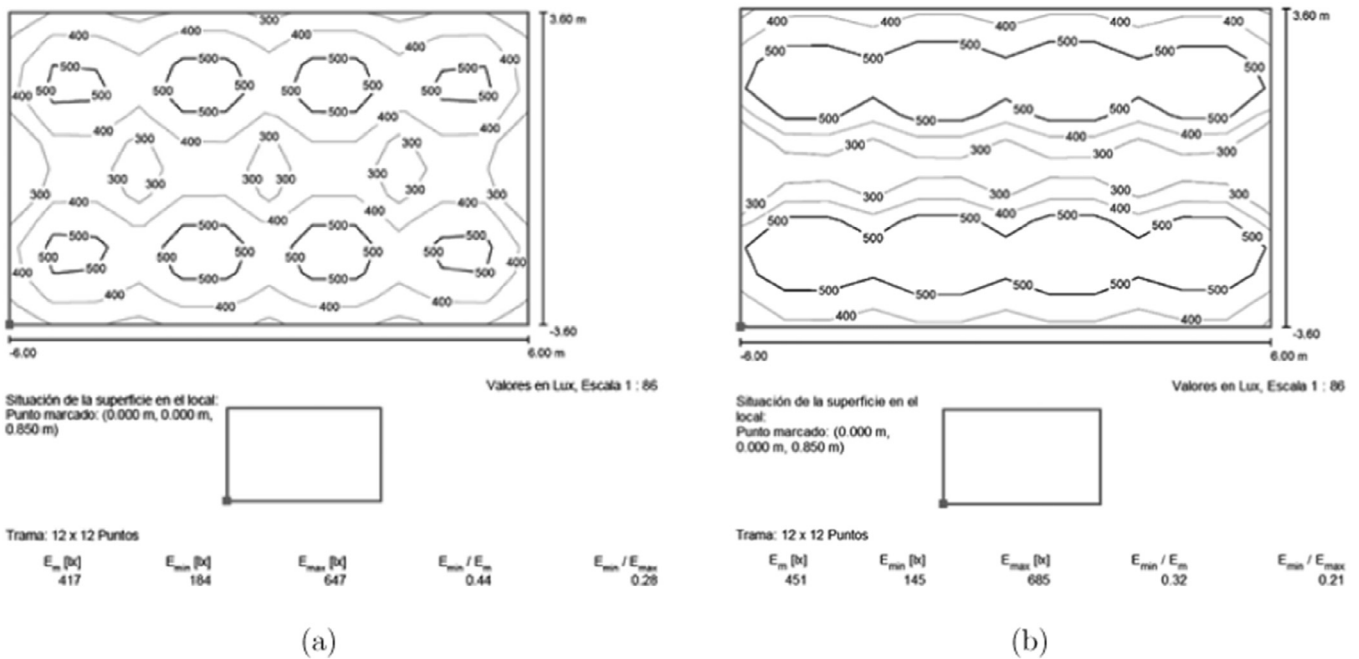
Fig. 15. Simulation result obtained with DIALux: (a) artificial lighting and (b) daylighting system.

Fig. 14 shows the interior layout of the office with a visualization of (a) artificial lighting calculations and (b) daylighting system calculations. Moreover, Fig. 15 shows a floor plan with the illumination levels obtained with both systems (C_2 configuration, June 21st and solar time 12:00). As can be seen, the mean illuminance, E_m, is higher with the daylighting system. On the contrary, the overall uniformity, E_{min}/E_m, is higher with artificial lighting.

5. Conclusions and future perspectives

Aspects of the design of a small scale linear Fresnel reflector applied to a daylighting system based on optical fiber bundles have been analyzed in this paper.

The study shows the influence of the numerical aperture of the optical fiber on the parameters of the SSLFR: mirror width, number of mirrors at each side of the central mirror, and distance between the OFB and the mirrors. The use of optical fibers with a small numerical aperture requires a smaller mirror width. The mirror width can be increased by increasing the distance between the mirrors and the optical fiber, but this solution is not recommended as it tends to reduce the optical efficiency of the collector. The mirror width can also be increased by decreasing the number of mirror, which would decrease the cost of the SSLFR. It was found that the Barbon method is suitable to determine the length and position of the OFB. The paper also addresses the preliminary design of a new reflector cavity for the SSLFR. This reflector cavity has two focal points, thus increasing the number of solar rays that impinge on the OFB. Optical simulations were performed to evaluate the optical efficiency of the proposed reflector cavity. Two configurations of the SSLFR, C_1 and C_2, were analyzed and the electric energy savings were evaluated for a typical office room. Finally, the light distribution was calculated using the lighting design software DIAlux, and the illumination level obtained with the daylighting system was compared with that of artificial lighting.

The originality of this work is based on two novel contributions: The design of a new daylighting system based on OFBs using an SSLFR, and the design of a new reflector cavity, since the cavity used in a conventional SSLFR is not suitable for this application.

Future work will entail the study of the use of this daylighting system in applications used for multi-floor office buildings, underground stations, among other.

Acknowledgments

References

[1] IEA. Light's labour's lost. Policies for energy-efficient lighting. International Energy Agency; 2006.
[2] Lin H, Wang Q, Wang Y, Liu Y, Sun Q, Wennersten R. The energy-saving potential of an office under different pricing mechanisms – application of an agent-based model. Appl Energy 2017;202:248–58.
[3] Lowry G. Energy saving claims for lighting controls in commercial buildings. Energy Build 2016;133:489–97.
[4] Wana KKW, Li DHW, Pan W, Lam JC. Impact of climate change on building energy use in different climate zones and mitigation and adaptation implications. Appl Energy 2012;97:274–82.
[5] Bodart M, de Herde A. Global energy savings in offices buildings by the use of daylighting. Energy Build 2002;34(5):421–30.
[6] Wong IL. A review of daylighting design and implementation in buildings. Renew Sust Energy Rev 2017;74:959–68.
[7] Al-Obaidi KM, Munaaim MAC, Ismail MA, Rahman AMA. Designing an integrated daylighting system for deep-plan spaces in Malaysian low-rise buildings. Solar Energy 2017;149:85–101.
[8] Das A, Kumar Paul S. Artificial illumination during daytime in residential buildings: factors, energy implications and future predictions. Appl Energy 2015;158:65–85.
[9] Wong I, Yang HX. Introducing natural lighting into the enclosed lift lobbies of highrise buildings by remote source lighting system. Appl Energy 2012;90:225–32.
[10] Belzer DB, Stanton WH, Shih-Miao C. Impact of extended daylight saving time on national energy consumption: technical documentation, prepared for U.S. Department of Energy, Office of Energy Efficiency and Renewable Energy; 2008.
[11] Hraska J. Chronobiological aspects of green buildings daylighting. Renew Energy 2015;73:109–14.
[12] Kim G, Kim JT. Healthy-daylighting design for the living environment in apartments in Korea. Build Environ 2010;45:287–94.
[13] Muhs JD. Design and analysis of hybrid solar lighting and full-spectrum solar energy systems. Presented at The American Solar Energy Society's, Solar 2000 conference, Wisconsin; 2000.
[14] Hafez AZ, Soliman A, El-Metwally KA, Ismail IM. Design analysis factors and specifications of solar dish technologies for different systems and applications. Renew Sust Energy Rev 2017;67:1019–36.
[15] Han H, Kim JT. Application of high-density daylight for indoor illumination. Energy 2010;35:2654–66.
[16] Ali IMS, O'Donovan TS, Reddy KS, Mallick TK. An optical analysis of a static 3-D solar concentrator. Solar Energy 2013;88:57–70.
[17] Jebasingh VK, Joselin Herbert GM. A review of solar parabolic trough collector. Renew Sust Energy Rev 2016;54:1085–91.
[18] Ullah I, Shin S. Highly concentrated optical fiber-based daylighting systems for multi-floor office buildings. Energy Build 2014;72:246–61.
[19] Renzi M, Cioccolanti L, Barazza G, Egidi L, Comodi G. Design and experimental test of refractive secondary optics on the electrical performance of a 3-junction cell used in CPV systems. Appl Energy 2017;185:233–43.
[20] Vu NH, Shin S. A large scale daylighting system based on a stepped thickness waveguide. Energies 2016;71:1–15.
[21] Kim Y, Jeong HJ, Kim W, Chun W, Han HJ, Lim SH. A comparative performance analysis on daylighting for two different types of solar concentrators: Dish vs. Fresnel lens. Energy 2017;137:449–56.
[22] López G, Gueymard CA. Clear-sky solar luminous efficacy determination using artificial neural networks. Solar Energy 2007;81:929–39.
[23] CIE. Photometry - the CIE system of physical photometry. Publ CIE S 010/E:2004, Commission Internationale de l'Eclairage, Central Bureau, Vienna; 2004.
[24] Cucumo M, De Rosa A, Ferraro V, Kaliakatsos D, Marinelli V. Correlations of direct solar luminous efficacy for all sky, clear sky and intermediate sky conditions and comparisons with experimental data of five localities. Renew Energy 2010;35:2143–56.
[25] Konga HJ, Kimb JT. Evaluation of global vertical illuminance and irradiance models against data from Yongin, South Korea. Energy Build 2015;91:139–47.
[26] Robledo L, Soler A. Luminous efficacy of direct solar radiation for clear skies. Energy 2000;25(8):689–701.
[27] Robledo L, Soler A. Luminous efficacy of direct solar radiation for all sky types. Energy 2001;26(7):669–77.
[28] Aydinli S, Krochmann J. Data on daylight and solar radiation: guide on daylight. Draft for CIE TC 4.2, Commission Internationale de l.Eclairage, Paris; 1983.
[29] De Souza RG, Robledo L, Soler A, Pereira FOR. Clear sky and all sky direct luminous efficacies for Florianopolis, Brazil. Energy Convers Manage 2005;46(3):361–71.
[30] Darula S, Kittler R, Gueymard AC. Reference luminous solar constant and solar illuminance for illuminance calculations. Solar Energy 2005;79:559–6511.
[31] Zain-Ahmed A, Sopian K, Zainol Abidin Z, Othman MYH. The availability of daylight from tropical skies—a case study of Malaysia. Renew Energy 2002;25:21–30.
[32] Muneer T. Solar radiation and daylight models. Elsevier; 2004.
[33] Chong KK, Onubogu NO, Yew TK, Wong CW, Tan WC. Design and construction of active daylighting system using two-stage non-imaging solar concentrator. Appl Energy; 2017. doi:http://dx.doi.org/10.1016/j.apenergy.2017.05.188.
[34] Barbón A, Barbón N, Bayón L, Otero JA. Theoretical elements for the design of a small scale linear Fresnel reflector: frontal and lateral views. Solar Energy 2016;132:188–202.
[35] Barbón A, Barbón N, Bayón L, Otero JA. Optimization of the length and position of the absorber tube in small-scale linear Fresnel concentrators. Renew Energy 2016;99:986–95.
[36] Kandilli C, Turkoglu AK, Ulgen K. Transmission performance of fibre-optic bundle for solar lighting. Int J Energy Res 2009;33(2):194–204.
[37] Franz JH, Jain VK. Optical communications: components and systems. CRC Press; 2000.
[38] Feuermann D, Gordon JM, Huleihil M. Light leakage in optical fibers: experimental results, modeling and the consequences for solar concentrators. Solar Energy 2002;72:195–204.
[39] Rahou M, Mojiri A, Rosengarten G, Andrews J. Optical design of a Fresnel concentrating solar system for direct transmission of radiation through an optical fibre bundle. Solar Energy 2016;124:15–25.
[40] Earl DD, Muhs JD. Preliminary results on luminaire designs for hybrid solar lighting systems. Presented at The American Society of mechanical engineers, forum 2001: solar energy, Washington, DC; 2001.
[41] Earp AA, Smith GB, Franklin J, Swift P. Optimisation of a three-colour luminescent solar concentrator daylighting system. Solar Energy Mater Solar Cells 2004;84:411–26.
[42] Tsangrassoulis A, Doulos L, Santamouris M, Fontoynont M, Maamari F, Wilson M, et al. On the energy efficiency of a prototype hybrid daylighting system. Solar Energy 2005;79:56–64.
[43] Schlegel GO, Burkholder FW, Klein SA, Beckman WA, Wood BD, Muhs JD. Analysis of a full spectrum hybrid lighting system. Solar Energy 2004;76:359–68.
[44] Reda I, Andreas A. Solar position algorithm for solar radiation applications. Technical report NREL/TP-560-34302, Colorado, USA; 2008.
[45] Theunissen P-H, Beckman WA. Solar transmittance characteristics of evacuated tubular collectors with diffuse back reflectors. Solar Energy 1985;35:311–20.
[46] Mathur SS, Kandpal TC, Negi BS. Optical design and concentration characteristics of linear Fresnel reflector solar concentrators – I. Mirror elements of varying width. Energy Convers Manage 1991;31(3):205–19.
[47] Mathur SS, Kandpal TC, Negi BS. Optical design and concentration characteristics of linear Fresnel reflector solar concentrators – II. Mirror elements of equal width. Energy Convers Manage 1991;31(3):221–32.
[48] Thorlabs. Technical data. < https://www.thorlabs.com > [accessed on: 6 June 2017].
[49] Shanmugapriya Balaji, Reddy KS, Sundararajan T. Optical modelling and performance analysis of a solar LFR receiver system with parabolic and involute secondary reflectors. Appl Energy 2016;179:1138–51.
[50] Duffie JA, Beckman WA. Solar engineering of thermal processes. 4th ed. John Wiley & Sons; 2013.
[51] Sharma VM, Nayak JK, Kedare SB. Comparison of line focusing solar concentrator fields considering shading and blocking. Solar Energy 2015;122:924–39.
[52] AAE. Agencia Andaluza de la Energía; 2017. < https://www.agenciaandaluzadelaenergia.es/Radiacion/radiacion1.php > .
[53] Barbón A, Barbón N, Bayón L, Sánchez-Rodríguez JA. Parametric study of the small scale linear Fresnel reflector. Renew Energy 2018;116:64–74.
[54] Mayhoub M, Carter D. A feasibility study for hybrid lighting systems. Build Environ 2012;53:83–94.
[55] EN 12464-1:2003: light and lighting - lighting of work places – Part 1: Indoor work places; 2003.
[56] Philips. Technical data. < http://www.lighting.philips.com/home > [accessed on: 6 June 2017].
[57] DIAL GmbH. Light building software. < http://www.dial.de/es/home > [accessed on: 4 November 2017].
[58] Salata F, Golasi I, Salvatore M, Lieto Vollaro A. Energy and reliability optimization of a system that combines daylighting and artificial sources. A case study carried out in academic buildings. Appl Energy 2016;169:250–66.